Deep Learning Time Series Prediction Strategies for Efficiently Emulating Noah Land Surface Model Soil Moisture Dynamics

Mitchell T. Dodson

A THESIS

Submitted in partial fulfillment of the requirements
for the degree of Master of Science in Atmospheric Science
in
The Department of Atmospheric and Earth Science
to
The Graduate School
of
The University of Alabama in Huntsville

May 2025

Approved by:

Dr. Christopher Hain, Research Advisor
Dr. Sundar Christopher, Committee Chair
Dr. Sean Freeman, Committee Member
Dr. Lawrence Carey, Department Chair
Dr. [College Dean Name], College Dean
Dr. Jon Hakkila, Graduate Dean

Abstract

Deep Learning Time Series Prediction Strategies for Efficiently Emulating Noah Land Surface Model Soil Moisture Dynamics

Mitchell T. Dodson

A thesis submitted in partial fulfillment of the requirements for the degree of Master of Science in Atmospheric Science

Atmospheric and Earth Science

The University of Alabama in Huntsville

May 2025

This work examines the ability of deep learning time series generative models to accurately and efficiently emulate the hourly temporal dynamics of the Noah Land Surface Model (Noah-LSM) out to a 2 week forecast horizon, given atmospheric forcings and static parameterization provided by the second phase North American Land Data Assimilation System (NLDAS-2) framework. Results from multiple neural network architectures are compared alongside variations in prediction target, loss function characteristics, and model properties. The most performant model types are subsequently evaluated with respect to forecast distance, daily and annual seasonality, and against a variety of regional scenarios, including several extreme event case studies. Ultimately, we present a software system for developing and testing neural networks that use time-varying and static data to estimate temporal dynamics, with the goal of providing a foundation for similar data-driven modeling techniques to be implemented within the upcoming third phase of the NLDAS data record.

Acknowledgements

You must pay your scholarly debts by thanking those who have provided intellectual guidance, facilities, or financial support for your project; thus, you thank those who have been significantly involved in your work. You must acknowledge any agency providing funding or other resources, and any individual or institution who has granted you permission to reprint material.

If you wish, you may also thank family or friends. You may conclude your acknowledgments with a dedication rather than using a separate dedication page. Your acknowledgments should be brief and consistent in tone with a formal publication.

Table of Contents

List of Figures

List of Tables

Chapter 1. Introduction

Accurate characterization of the distribution of water content within the soil column by land surface models is critical for governing land-atmosphere interaction in numerical weather prediction (NWP) (Brocca et al., 2010) (Koster et al., 2010), operational decision making preceding and during drought and flood events (Otkin et al., 2016), and for downstream datasets aiding assessment of vegetation health, crop yield prediction, and fire risk characterization (Case et al., 2023). In order to address these needs, the Noah-LSM was developed to serve as the land surface component coupled to NWP models including the Weather Research and Forecasting Model (WRF), the Global Forecast System (GFS) (Jin et al., 2010) (Mitchell et al., 2005), and climate models including the NCEP Climate Forecast System (CFSv2) (Saha et al., 2014). Noah-LSM also aids National Weather Service forecasts and US Drought Monitor designations within decision support frameworks like the Short-Term Research, Prediction, and Transition high-resolution implementation of the Land Information System (SPoRT-LIS) (Case et al., 2022) (Case and White, 2014), and facilitates research and derived product development by providing soil states for NASA Land Data Assimilation System (LDAS) datasets (Ek et al., 2003).

By applying observational and reanalysis data to Noah and other land surface models, NLDAS has provided the community with consistent and quality-controlled multi-model land surface states and associated forcings in a near real-time capacity since 1999 (Cosgrove et al., 2003), with phase 2 of the project also contributing a retrospective climatology extending back to 1979. The first and second generation data products are calculated on a 1/8 degree geodetic grid spanning land-dominated points in the conterminous United States (CONUS) from 25° to 53° North latitude and 125°-67° West longitude, and are released at an hourly frequency (Mitchell et al., 2004) (Xia et al., 2012b). The third phase of the data assimilation system is currently under development, and aims to implement a wealth of upgrades including new data assimilation techniques and physical parameterizations, an increase in the spatial resolution to $1km^2$, and the expansion of the domain to the full North American continent. As a consequence, the total number of valid land grid cells will increase dramatically from 76,088 in the first two phases to 27,245,580 with NLDAS-3 data products. In addition to the larger domain and updated physical processes used to develop the forcings and land surface states, the NLDAS-3 data suite will feature a variety of derived products. These products are anticipated include gridded climatological anomaly and segmented percentile data, stream routing and discharge estimates, and ensemble mean and spread information using forecast forcings (Kumar et al., 2024).

As the domain size and sophistication of data assimilation systems and land surface models like NLDAS and Noah-LSM continues to grow, a niche de-

velops for methods that can generate reasonable estimates of the dynamics of numerical models which require less compute time, simplify the runtime environment of the program, and which can be fitted to observational data and then generalized to broader domains without accruing significant additional complexity to the parameterization scheme. Data-driven modeling techniques like deep learning with artificial neural networks (ANNs) are addressing this need by introducing the ability to approximate the highly nonlinear and conditional relationships between arbitrary predictor and target datasets. This flexibility is accomplished by learning a sequence of transformations which are encoded as a composition of alternating high-dimensional matrix operations and element-wise nonlinear functions, and which serve as a mapping from the vector of predictors to a corresponding target vector (Hornik et al., 1989).

In the context of time series physical modeling, ANNs enable the development of a statistically optimal approximation of the relationship between past states, simultaneous covariate data variables, and unknown current or future states. This general principle has a wealth of use cases. Previous literature shows that ANNs are computationally efficient and reasonably accurate for modeling dynamical systems like Lorenz'95 by formulating the problem as a discrete-time estimator of an ordinary differential equation which isn't explicitly known by the model (Fablet et al., 2018). ANNs can also be structured to have useful properties like the ability to estimate the jacobian of the transfer mapping between inputs and future states, even if the system being emulated isn't differentiable (Nonnenmacher and Greenberg, 2021). The same strategy may be applied to

forecasting the evolution of datasets like ECMWF Reanalysis v5 (ERA5) in a local or global domain, however significant challenges emerge as (Dueben and Bauer, 2018) identify. As they describe, ANNs cannot be constrained by default to conserve quantities like energy and water, and unlike numerical models, their handling of the underlying physical processes as a "black-box" mean that identifying sources of error within the model is difficult and often speculative. Furthermore, Earth system data tend to be highly regionally variable (ex. vegetation types), exhibit nonlinear autocorrelation between multiple variables (ex. temperature, dewpoint, and cloud cover), and are subject to rare but influential outliers (ex. snow and extreme precipitation). As such, although ANNs are adept at handling very nonlinear and conditional problem types, achieving the best performance and interpretability requires the utilization of application-specific knowledge when constructing and evaluating deep learning models.

Within the field of hydrologic modeling, most of the recent literature applying deep learning methods has focused on rainfall-runoff problems, where models forecast the hydrograph of a stream given time-varying atmospheric and land surface states as well as static properties. Inputs are typically considered within a spatial boundary drawn from a watershed outlet where a streamflow station provides the prediction target by directly observing the discharge. To that end, (Kratzert et al., 2018) applies a particular ANN architecture called Long Short-Term Memory (LSTM) networks to modeling discharge from the CAMELS dataset (Addor et al., 2017), which contains daily-resolution streamflow and meteorological forcings alongside parameters describing the topographic, land use, soil,

and geologic properties of 671 catchments. They show that models trained on single basins often outperform models trained using data from multiple basins within a region, and that subsequent "fine-tuning" of a generalized regional model on individual basins slightly improves model efficiency in many cases. Later, (Kratzert et al., 2019) improves on LSTM model performance by modifying the training strategy to optimize an objective function similar to Nash-Sutcliffe Efficiency (Nash and Sutcliffe, 1970), and by introducing a modification to the architecture that allows for static catchment parameters to be separately provided – and their influence separately investigated – from time-varying inputs. These experiments even out-performed several process-based models that were tuned specifically to the individual test basins. In spite of their black-box nature, (Lees et al., 2022) demonstrates that LSTMs used for daily-scale rainfall-runoff prediction maintain information correlated with physical properties of the catchment's hydrologic state including soil moisture and snow cover, which indicates that they preserve meaningfully interpretable data about their inputs. The general approach of employing LSTMs for discharge forecasting is already being utilized by stakeholders like the United States National Weather Service and River Forecast Center offices in an operational setting with the NASA SPoRT Streamflow-AI product, which uses near real-time Noah-LSM soil moisture estimates and outlooks as an input via the SPoRT-LIS data product (White et al., 2025), (Case et al., 2022).

Relatively few publications have applied deep learning techniques to estimate soil dynamics over a consistently spatially gridded domain, akin to the outputs of process-based models like Noah-LSM. In one instance, (Filipović et al.,

2022) applied LSTMs to global daily-scale ERA5 data in order to predict the 3-day evolution of moisture content in an intermediate-depth soil layer. This is conceptually similar to emulating Noah-LSM using NLDAS forcings because ERA5 determines its soil moisture states using the ECMWF Scheme for Surface Exchanges over Land (Balsamo et al., 2009). Additionally, (O. and Orth, 2021) used an LSTM to assist in generalizing in-situ observations at 3 soil depth levels to a regional grid, also using daily ERA5 forcings data as an input, and adjusting predictions to match the pixel-wise gaussian parameters of the ERA5 soil moisture analysis. Both of these approaches use long lead times of 60 days or 1 year, respectively, and make predictions at only a few forecast horizons per execution of the model (3 days and 1 day, respectively).

This work seeks to apply a similar strategy of data-driven modeling for hourly-scale emulation of Noah-LSM over the full NLDAS-2 grid domain, with the goal of generating accurate and computationally reasonable forecasts out to a two-week horizon at three depth levels simultaneously. We will construct a few distinct neural network types suited to this problem structure, compare their results through a variety of bulk statistics and case studies using physical reasoning, discuss lessons learned regarding training methodology, and present a general free and open-source framework for developing time series dynamical estimators using deep learning for gridded physical datasets.

Chapter 2. Background

In this chapter we will elaborate on the history and relevant details of the implementation of NLDAS and Noah-LSM, frame the problem in terms of the difference between numerical modeling and data-driven modeling approaches, and describe the technical properties and pertinent considerations for neural networks intended for time series modeling.

2.1 NLDAS and Noah-LSM: History and Implementation

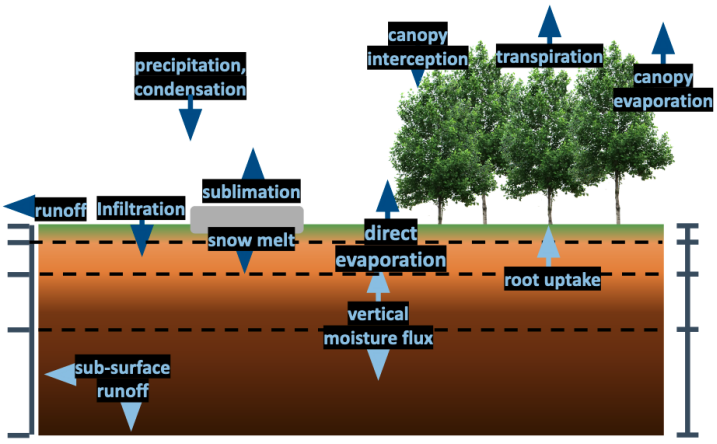

Figure 2.1: Schematic diagram of the feedbacks contributing to the evolution of soil moisture in Noah-LSM

The theoretical framework underpinning Noah-LSM was initially formulated in the 1980s as part of the OSU model, which characterizes boundary layer

moisture and energy fluxes as a 2-layer soil model subject to atmospheric forcings. The model expresses the infiltration and movement of water between the soil layers with the diffusive form of the Richards equation (Mahrt and Pan, 1984), direct evaporation using an analytic approximation of the Penman-Montieth relation in terms of atmospheric stability (Mahrt and Ek, 1984), and basic plant transpiration in terms of vegetation density and soil water content (Pan and Mahrt, 1987). These features form an interdependent system of differential equations that are numerically integrated using a combination of the Crank-Nicholson method and finite-differencing (Chen et al., 1997), which introduces the need for short time steps of 15 or 30 minutes in order for the system to remain numerically stable (Cartwright and Piro, 1992)(Mahrt and Pan, 1984).

The OSU model was later significantly improved, renamed to the first generation of Noah-LSM, and coupled with the NCEP Eta forecast model. Noah-LSM expanded the domain to four soil layers of increasing thicknesses (10cm, 30cm, 60cm, and 100cm), improved runoff dynamics by implementing Philip's equation for infiltration capacity (Schaake et al., 1996), and represented the influence of soil texture on moisture transport by introducing bounds on bare-soil potential evaporation that are determined by the soil composition (Betts et al., 1997) (Mahfouf and Noilhan, 1991). The model also features a significantly enhanced representation of vegetation including a more thorough treatment of canopy resistance via a "Jarvis-type" model of leaf stomatal control (Jarvis et al., 1976) (Jacquemin and Noilhan, 1990), which accounts for the dependence of transpiration on insolation, air temperature and dewpoint, soil moisture content, and vegetation density.

The vegetation effects are scaled by a monthly climatology of normalized difference vegetation index (NDVI) values observed by the NOAA-AVHRR satellite radiometer, which serve as a proxy for green vegetation fraction (GVF) (Gutman and Ignatov, 1998) (Chen et al., 1996), and the depth of root water uptake associated with plant transpiration is determined by a pixel's vegetation class as specified by the Simple Biosphere Model (Dorman and Sellers, 1989). Finally, the model's utility was greatly expanded with the addition of a frozen soil and snow pack parameterization incorporating the thermal and hydraulic properties of fractionally-frozen soil layers, the effects of state changes (Chen et al., 1996) (Koren et al., 1999), radiative feedbacks from partial snowpack coverage, and a snow density scheme (Ek et al., 2003).

Soon after the turn of the millennium, the first generation of NLDAS was under development as part of a multi-institution collaborative effort sponsored by the Global Energy and Water Cycle Experiment (GEWEX) Continental-scale International Projects (GCIP) team. The goal of the project was to incorporate long-term observations of land surface temperature, snow pack depth, and meteorological forcings from multiple sources (in-situ, satellite, radar) into a common framework used to independently evaluate land surface states and energy fluxes with four land surface models including Noah-LSM (Mitchell et al., 2004). Over a domain including the full conterminous United States (CONUS) at 0.125° resolution, the models were allowed to spin up over the course of a year, and soil states were recurrently used to initialize subsequent time steps rather than being "nudged" to correct for drift. Land cover and soil texture classification over the

domain was derived by coarsening the University of Maryland and STATSGO datasets, respectively, from their native 1km resolutions (Hansen et al., 2000), surface geometry and elevation is provided by the GTOPO30 dataset (of the Interior, 1997), and the parameter values for soil hydraulic properties were adapted from observations taken at the University of Virginia (Cosby et al., 1984).

Attention remained on Noah-LSM in the following years as it continued to support NLDAS and other data assimilation and forecasting systems, which led to a series of improvements introduced alongside the next phase of the NLDAS project. A seasonal effect was added to vegetation by scaling the leaf area index (LAI) by the GVF within bounds determined by the plant type, and transpiration was scaled by a root uptake efficiency factor determined by the proximity of soil temperature to an optimum growth temperature (298 K). Several parameters were adjusted including the influence of vapor pressure deficit on transpiration rate, the minimum stomatal resistance for several plant species, and hydraulic parameters for some soil textures. The aerodynamic conductance coefficient – an important factor in the strength of moisture and energy fluxes from the surface – was increased during daylight hours, and a basic anisotropy model was introduced by modifying the albedo of some surfaces in terms of the solar zenith angle (Wei et al., 2011). Snowpack physics were also modified to improve surface exchange coefficients, and to gradually diminish the snow albedo over the time since the last snowfall (Livneh et al., 2010) (Liang et al., 1994). These changes introduce new feedbacks and involve sensitive parameters like LAI which have a strong influence on the model's dynamics (Rosero et al., 2010). The retrospective NLDAS-2 data

Forcing	Unit	Source	Δt	Δx
Precipitation	kg m^{-2}	CPC Gauge observations	24h	14km
		WSR-88D retrievals	1h	4km
Temperature	K	NCEP NARR	3h	32km
Specific Humidity	kg kg^{-1}	NCEP NARR	3h	32km
Surface Pressure	Pa	NCEP NARR	3h	32km
Wind Velocity	m s^{-1}	NCEP NARR	3h	32km
Incident LW Flux	W m^{-2}	NCEP NARR	3h	32km
Incident SW Flux	W m^{-2}	GOES, NARR	3h, 1h	14km
Green Veg Fraction	%	AVHRR NDVI	Monthly	16km
Leaf Area Index	m^2 m^{-2}	UMD, AVHRR NDVI	Monthly	16km

Table 2.1: Atmospheric forcings and other time-varying parameters provided by NLDAS-2 at a 1-hourly resolution on the 0.125° CONUS grid. Data are resampled using spatial bilinear interpolation, then temporal disaggregation according to (Cosgrove et al., 2003). NLDAS forcing files also include values for convective available potential energy, the ratio of precipitation from convection, and surface potential evaporation (calculated as in Mahrt and Ek (1984)), but these three values aren't currently used as inputs to the models.

record generated after applying these modifications extends back to 1979, and continues to be updated in a near real-time capacity (Xia et al., 2012b).

The NLDAS-2 time-varying retrospective forcings listed in Table 2.1 will serve as the predictors used by the neural networks to forecast the Noah land surface model soil moisture states. Temperature, humidity, pressure, wind speed and heading, and longwave flux are derived exclusively from the National Centers for Environmental Prediction (NCEP) North American Regional Reanalysis (NARR) data product. As part of the downscaling procedure from their native 32km resolution to the 1/8° NLDAS domain, a lapse rate adjustement is applied to the temperature and humidity fields based on the elevation profile. Downward shortwave radiative flux is calculated using a blend of NARR and hourly Geostationary Operational Environmental Satellite (GOES) data, with a ratio-based bias correction based on (Berg et al., 2003) applied to account for a known positive bias in NARR-reported downward shortwave flux, and to mitigate discontinuities arising from the merger the two data sources (Pinker et al., 2003) (Xia et al., 2012a). Precipitation receives a special treatment in order to ensure sufficient spatial resolution and consistency; the Climate Prediction Center (CPC) daily gauge-based product (Chen et al., 2008) serves as the baseline, which is temporally disaggregated to 1 hour resolution using National Weather Service WSR-88D radar retrievals (Fulton et al., 1998). In regions lacking radar coverage, the disaggregation is completed using a weighted combination of the CPC's satellite-derived estimates from morphed passive-microwave and infrared observations (CMORPH) (Joyce et al., 2004), and the CPC Hourly Precipitation

Dataset (HPD), with NARR data as a final fallback (Baldwin and Mitchell, 1997). Although both the LAI and GVF vegetation parameters are based on multi-year monthly averages, they are disaggregated to an hourly resolution in order to be smoothly variable (Wei et al., 2011), and are thus treated like an atmospheric forcing in this work.

2.2 Distinctions in Modeling Techniques

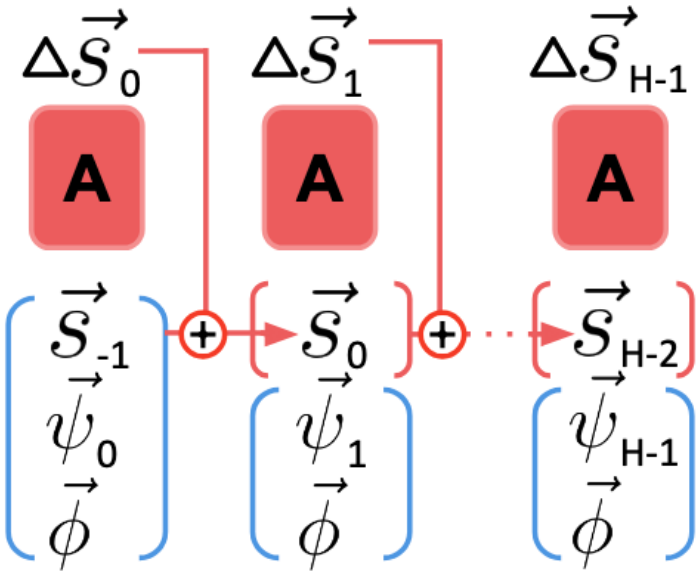

Figure 2.2: Diagram of a self-cycling discrete-time dynamical system with no hidden state. At each time, nonlinear operator **A** maps an initial state $\vec{s}_k$, exogenous forcing $\vec{\psi}_k$, and time-invariant parameters $\vec{\phi}$ to a new state $\Delta\vec{s}_{k+1}$, used to initialize the subsequent time step, and so forth until H predictions have been made. As a matter of convention, time step zero refers to the first perturbation of the initial state after applying the model's first increment change estimate, and includes the forcings that informed that perturbation.

2.2.1 Noah-LSM as a Discrete Dynamical System

At its core, Noah-LSM is a collection of coupled differential equations that express the total derivative of land surface states $\frac{d\vec{s}}{dt}$ in terms of the current state $\vec{s}$, forcing $\vec{\psi}$, and time-invariant properties of each grid cell $\vec{\phi}$. Since the model is implemented as an algorithmic procedure and is not continuously differentiable, we will use the notation $\frac{\Delta\vec{s}_k}{\Delta t} \approx \mathbf{A}(\vec{s}_{k-1}, \vec{\psi}_k, \vec{\phi}_k, \Delta t)$ to refer to the model as a transition function evaluated at a discrete time step Δt, such that the system evolves as a dynamical system described by Equation 2.1.

$$\vec{s}_k = \vec{s}_{k-1} + \mathbf{A}(\vec{s}_{k-1}, \vec{\psi}_k, \vec{\phi}_k, \Delta t) \cdot \Delta t \tag{2.1}$$

Here, $\vec{s}$ refers to the model's dynamic state variables like snow pack depth, soil moisture and temperature, and canopy storage, $\vec{\psi}$ encodes the covariate atmospheric variables from Table 2.1 (which are derived from weather forecasts or observations), and $\vec{\phi}$ includes coefficients of the governing equations like vegetation type/fraction, soil texture, and slope/elevation.

To generate a time series, Noah-LSM numerically integrates the system of equations using Euler and Crank-Nicholson techniques, which explicitly evaluate the differential equations at several time intervals per computational time step in order to estimate the nonlinear change in state, which evolves continuously in the real system being modeled. It is crucial that the increment change in time remains small between evaluations of the model (15min for NLDAS-Noah) to

mitigate truncation error from the assumption of local linearity (Mitchell et al., 2004) (Cartwright and Piro, 1992).

2.2.2 Process-based vs Data-driven Models

The process-based approach of numerical models like Noah-LSM is practically and epistemologically distinct from data-driven techniques like deep learning. In a process-based paradigm, the inductive biases that govern the model's behaviors can be explicitly understood since they are based on a characterization of the physical system which is derived from theoretical knowledge. Some uncertainty is introduced by the input data, and is shared among all model types; this includes uncertainty from noise and interpolation of forcing observations, discrete treatment of surface types, etc. Aside from that, model error in process-based models arises from sources including inadequacy of the theory for describing the system (that is, phenomena which are neglected or misrepresented, and become a source of unexplained variance), and truncation error accumulated from the approximation techniques used to solve the model's governing equations. Explicit understanding of the reasons for the model's behavior has the advantage of being interpretable, in the sense that particular systems within the model can be independently evaluated and blamed for contributing uncertainty. Additionally, granting the ability to impose absolute constraints within the model structure ensures the outputs fully adhere to some physical requirements, such as conservation of water and energy. Nonetheless, the onus falls entirely on the model developer to adjust many details of the implementation of the processes. The act

of tuning a numerical model's parameters often implies postulating a source of uncertainty, addressing it by manually manipulating coefficients or introducing new systems within the governing equations, and then evaluating the impact of the changes using correlational analysis with a subset of the available data. This can be a laborious process, and typically results in the gradual accumulation of feedbacks and complexity within the model.

In contrast, many data-driven approaches to modeling physical systems – deep learning in particular – sacrifice the explainability and rigorous physicality of their estimates in exchange for developing a statistically optimal approximation of the relationship between the input and output domains by any means available. Although the overall algorithmic structure of the ANN is established by the developer – typically based on broad heuristics from past literature and experimentation – very little control can be asserted over the particular means by which predictions are determined from inputs. Instead, the effectiveness of the ANN's performance is characterized in terms of a differentiable loss function (also known as the objective or cost function) which may be defined by the developer, and which is fundamentally (though indirectly) important for determining the solution developed in the training phase.

An ANN's learnable parameters refer to the real-valued elements of a series of arbitrarily-sized square matrices encoding affine transformations. Each "layer" of the ANN is comprised of one of these affine transformations followed by an element-wise nonlinear operation on its output, and the full ANN typically consists of multiple layers which are combined via composition or any kind of

differentiable arithmetic operation. During training, all of the ANN's learnable parameters are iteratively adjusted by estimating the gradient of the loss function with respect to the parameters (given batched subsets of the predictor/target data pairs) then determining the direction and magnitude by which the parameters in each of the layers should be modified with an algorithm called backpropagation (Rumelhart et al., 1986). The general strategy of determining the sensitivity of the loss landscape to changes in the ANN's parameters, and tweaking them accordingly, is referred to as gradient descent. Given at least 2 layers (which constitutes the definition of a *deep* ANN), the network is theoretically capable of expressing an arbitrary decision boundary or multivariate function given a sufficient number of parameters (Hornik et al., 1989). This high level of expressivity enables the network to learn complex relationships and generalizations among high-dimensional parameters, given repeated exposure to instances of these relationships during training.

The principle of ANNs using high-dimensional nonlinear correlations rather than explicit processes to model the correspondence between two datasets is powerful because they can approximate a highly nonlinear regression without numerically integrating a complex algorithm, and they can learn their parameterization based on a large volume of data without manual intervention. The quintessential drawback of relying on a black-box approach, though, is that models may perform poorly for no apparent reason, or may perform well for a fraught reason. For example, in one commonly-invoked anecdote described by (Lapuschkin et al., 2019), an image classifier over-performing but failing to generalize at identifying horses

in a grassy field was found to actually rely on the presence of the watermark of a particular equestrian photographer whose work was a part of the training data. As such, only regarding bulk statistics and loss performance as indicative of a model's success is insufficient to consider it trustworthy. In a data-driven paradigm, then, the role of the ANN developer is to facilitate effective and reliable learning through careful training data curation, congnizant loss function and model architecture design, and thorough evaluation of the model's behavior in local and global scenarios throughout the input domain in order to ensure the effectiveness and consistency of predictions in a variety of inference settings.

Furthermore, it is important to note that in the current scope of this work, it is not possible for the ANNs to leverage their expressivity to out-perform the numerical model. Since the ANNs presented here are merely emulating the processes that are programmed into Noah-LSM, it isn't reasonable to expect the models to form a more accurate representation of real soil dynamics. Nonetheless, it is conceivable that future work could utilize a similar approach to (O. and Orth, 2021) in order to integrate observational data into the training domain alongside model data, or to use it as a prediction target. The merger of these two data sources could aid in improving a data-driven model beyond the limitations of a numerical model's structure.

2.3 Deep Learning of Time Series

The most simple variant of an ANN is referred to as a feed-forward neural network (FNN), which consists of a series of composed layers (see previous section)

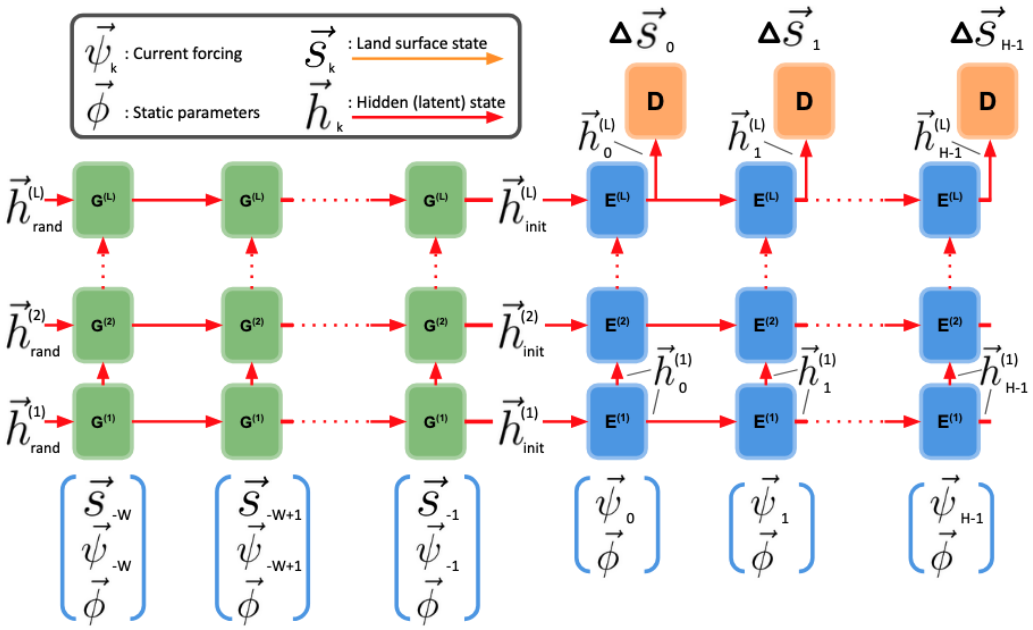

Figure 2.3: Schematic representation of an abstract sequence-to-sequence RNN with multiple layers. The architecture consists of L window encoder layers ($\mathbf{G}^{(1)}$-$\mathbf{G}^{(L)}$) incorporating context along the W spin-up window timesteps, L horizon encoder layers ($\mathbf{E}^{(1)}$-$\mathbf{E}^{(L)}$) generating H top-layer latent vectors corresponding to each of the prediction times, and 1 layer of decoder weights $\mathbf{D}$ which converts each of the top-layer latent vectors to a prediction for the increment change in state $\Delta\vec{s}$ between the current timestep and the next one. Parameters are shared across timesteps for each of $\mathbf{G}$, $\mathbf{E}$, and $\mathbf{D}$ individually, though each layer has distinct parameters.

mapping the input vector directly to the output. Although a FNN is theoretically capable of simulating Noah-LSM in the manner of Figure 2.2, inductive biases are commonly introduced in model architectures in order to promote efficiency, explainability, stability, and parsimony. For example, most neural networks used for sequence modeling like the recurrent neural networks (RNNs) in Figure 2.3 maintain one or more "hidden" latent parameters $\vec{h}$ with an arbitrary number of dimensions. This vector is modified and passed along by each subsequent iteration, giving the network the ability to make generalizations and propagate

information between time steps. Although $\vec{h}$ is typically difficult to interpret directly, the gradient descent process incentivizes the network to preserve and consolidate information that is needed to accurately generate the full sequence of predictions. Each of the following network architectures ultimately aim to improve the information quality of the latent vector by implementing algebraic structure, introducing statistical uncertainty, and encouraging sparsity.

$$\begin{aligned} \vec{h}_k^{(1)} &= \mathbf{E}^{(\mathbf{1})}\left(\vec{h}_{k-1}^{(1)},\, \vec{\psi}_k,\, \vec{\phi}\right) \\ \vec{h}_k^{(j)} &= \mathbf{E}^{(\mathbf{j})}\left(\vec{h}_{k-1}^{(j)},\, \vec{h}_k^{(j-1)}\right) \\ \vec{s}_{k+1} &= \vec{s}_k + \mathbf{D}\left(h_k^{(L)}\right) \end{aligned} \tag{2.2}$$

The RNNs discussed here will follow the structure described by Equation 2.2, which is consistent with the abstract architecture diagrammed in Figure 2.3.Here $\vec{h}_k^{(1)}$ is the first-layer latent vector given the static and dynamic inputs as well as the latent vector from the previous first-layer timestep, $\vec{h}_k^{(j)}$ is an intermediate-layer latent vector such that $j \in [2,\, L]$, and when $k = 0$ (the first horizon timestep), $\vec{h}_{-1}^{(s)} = \vec{h}_{\text{init}}^{(s)}$ for any layer s. The spin-up window layers prior to the first timestep ($\mathbf{G}^{(s)}$ in Figure 2.3) have their own sets of weights since the first-layer arguments include the known past soil states. Only the hidden states corresponding to the final timestep are captured from each layer of the spin-up window, and are exclusively used to provide historical information to the initial timesteps of the corresponding layers in the prediction horizon sequence. The accumulation step for calculating the new state $\vec{s}_{k+1}$ with the decoded prediction of

increment change in state also emphasizes another property of ANN-based models: unlike numerical models akin to the dynamical system described by Equation 2.1, the ANNs abstract away the concept of a variable increment time between input and prediction steps. Instead, the ANNs are trained to make predictions at a fixed timestep that cannot be changed during inference.

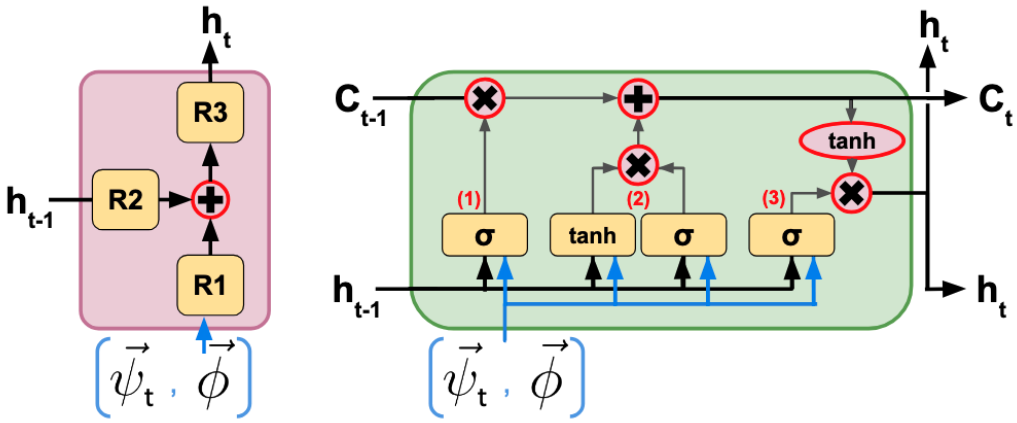

Figure 2.4: Schematic representation of individual RNN cells, the naïve RNN (left), and the LSTM (right)

The basic RNN architecture is vulnerable to the so-called vanishing or exploding gradient problem, which arises from the fact that $\vec{h}_k$ is the product of a learned matrix operation. Since the encoder and decoder weights are shared between sequence steps, the backpropagation through time algorithm may update a parameter many times per sample during training, which can cause weights to diverge and cease learning (Mozer, 1995). Furthermore, since the hidden state undergoes a nonlinear transformation at each step, it is difficult for the network to sustain information over a long context of past observations.

The LSTM architecture addresses these shortcomings by maintaining a separate hidden state $\vec{C}_t$ called the context vector. Rather than being generated by a matrix operation, the context vector is only modified by the output of a series of three "gates." These gates (numbered in Figure 2.4) include (1) the "forget gate", which uses a FNN to select a vector of values in the range (0,1). The vector is multiplied element-wise by $\vec{C}_{t-1}$ in order to selectively emphasize or diminish its activation. The "update gate" (2) transforms the inputs into a new coefficient vector in the range (-1,1), which is added to the context vector in order to retain information from the current time step. Finally, the "output gate" (3) generates a vector of multiplicative coefficients in the range (0,1) used to scale the new context vector $\vec{C}_t$ to the output latent state $\vec{h}_t$ **?**. The context vector remains stable compared to a hidden vector that is recurrently operated on by the same weight matrix, which facilitates the network to learn over a longer sequence interval.

Chapter 3. Data and Methodology

Table 3.1: Frequencies for equal-tempered scale, $A_4 = 440$ Hz. This table shows only the first five notes of a chromatic scale starting on C_0

Note	**Frequency (Hz)**	**Wavelength**
C_0	16.35	2109.89
$C_0^{\#}/D_0^b$	17.32	1991.47
D_0	18.35	1879.69
$D_0^{\#}/E_0^b$	19.45	1774.20
E_0	20.60	1674.62

References

Addor, N., Newman, A. J., Mizukami, N., and Clark, M. P. (2017). The CAMELS data set: catchment attributes and meteorology for large-sample studies. *Hydrology and Earth System Sciences*, 21(10):5293–5313. Publisher: Copernicus GmbH.

Baldwin, M. and Mitchell, K. (1997). The NCEP hourly multisensor US precipitation analysis for operations and GCIP research. *American Meteorological Society*, 54(Preprints, 13th Conference on Hydrology, Long Beach, CA):55.

Balsamo, G., Beljaars, A., Scipal, K., Viterbo, P., Hurk, B. v. d., Hirschi, M., and Betts, A. K. (2009). A Revised Hydrology for the ECMWF Model: Verification from Field Site to Terrestrial Water Storage and Impact in the Integrated Forecast System. *Journal of Hydrometeorology*, 10(3):623–643. Publisher: American Meteorological Society Section: Journal of Hydrometeorology.

Berg, A. A., Famiglietti, J. S., Walker, J. P., and Houser, P. R. (2003). Impact of bias correction to reanalysis products on simulations of North American soil moisture and hydrological fluxes. *Journal of Geophysical Research: Atmospheres*, 108(D16). _eprint: https://onlinelibrary.wiley.com/doi/pdf/10.1029/2002JD003334.

Betts, A. K., Chen, F., Mitchell, K. E., and Janjić, Z. I. (1997). Assessment of the Land Surface and Boundary Layer Models in Two Operational Versions of the NCEP Eta Model Using FIFE Data. *Monthly Weather Review*, 125(11):2896–2916. Publisher: American Meteorological Society Section: Monthly Weather Review.

Brocca, L., Melone, F., Moramarco, T., and Morbidelli, R. (2010). Spatial-temporal variability of soil moisture and its estimation across scales. *Water Resources Research*, 46(2). _eprint: https://onlinelibrary.wiley.com/doi/pdf/10.1029/2009WR008016.

Cartwright, J. H. E. and Piro, O. (1992). THE DYNAMICS OF RUNGE–KUTTA METHODS. *International Journal of Bifurcation and Chaos*, 02(03):427–449.

Case, J. L., Schultz, C. J., and Hain, C. R. (2023). Role of Antecedent Soil Moisture and Vegetation Stress in Lightning-Initiated Wildfires. NTRS Author Affiliations: Ensco (United States), Marshall Space Flight Center NTRS Meeting Information: 103rd American Meteorological Society Annual Meeting; 2023-01-08 to 2023-01-12; undefined NTRS Document ID: 20230000164 NTRS Research Center: Marshall Space Flight Center (MSFC).

Case, J. L. and White, K. D. (2014). Assessment of the 3-km SPoRT Land Information System for Drought Monitoring and Hydrologic Forecasting. Technical report, NASA Martial Space Flight Center.

Case, J. L., White, K. D., Fuell, K. K., and Hain, C. R. (2022). NASA SPoRT Land Information System Products for Soil Moisture Analysis.

Chen, F., Janjic, Z., and Mitchell, K. (1997). Impact of Atmospheric Surface-layer Parameterizations in the new Land-surface Scheme of the NCEP Mesoscale Eta Model. *Boundary Layer Meteorology*, 85(3):391–421. Num Pages: 391-421 Place: Dordrecht, Netherlands Publisher: Springer Nature B.V.

Chen, F., Mitchell, K., Schaake, J., Xue, Y., Pan, H.-L., Koren, V., Duan, Q. Y., Ek, M., and Betts, A. (1996). Modeling of land surface evaporation by four schemes and comparison with FIFE observations. *Journal of Geophysical Research: Atmospheres*, 101(D3):7251–7268. _eprint: https://onlinelibrary.wiley.com/doi/pdf/10.1029/95JD02165.

Chen, M., Shi, W., Xie, P., Silva, V. B. S., Kousky, V. E., Wayne Higgins, R., and Janowiak, J. E. (2008). Assessing objective techniques for gauge-based analyses of global daily precipitation. *Journal of Geophysical Research: Atmospheres*, 113(D4). _eprint: https://onlinelibrary.wiley.com/doi/pdf/10.1029/2007JD009132.

Cosby, B. J., Hornberger, G. M., Clapp, R. B., and Ginn, T. R. (1984). A Statistical Exploration of the Relationships of Soil Moisture Characteristics to the Physical Properties of Soils. *Water Resources Research*, 20(6):682–690. _eprint: https://onlinelibrary.wiley.com/doi/pdf/10.1029/WR020i006p00682.

Cosgrove, B. A., Lohmann, D., Mitchell, K. E., Houser, P. R., Wood, E. F., Schaake, J. C., Robock, A., Marshall, C., Sheffield, J., Duan, Q., Luo, L., Higgins, R. W., Pinker, R. T., Tarpley, J. D., and Meng, J. (2003). Real-time and

retrospective forcing in the North American Land Data Assimilation System (NLDAS) project. *Journal of Geophysical Research: Atmospheres*, 108(D22). _eprint: https://onlinelibrary.wiley.com/doi/pdf/10.1029/2002JD003118.

Dorman, J. L. and Sellers, P. J. (1989). A Global Climatology of Albedo, Roughness Length and Stomatal Resistance for Atmospheric General Circulation Models as Represented by the Simple Biosphere Model (SiB). *Journal of Applied Meteorology and Climatology*, 28(9):833–855. Publisher: American Meteorological Society Section: Journal of Applied Meteorology and Climatology.

Dueben, P. D. and Bauer, P. (2018). Challenges and design choices for global weather and climate models based on machine learning. *Geoscientific Model Development*, 11(10):3999–4009.

Ek, M. B., Mitchell, K. E., Lin, Y., Rogers, E., Grunmann, P., Koren, V., Gayno, G., and Tarpley, J. D. (2003). Implementation of Noah land surface model advances in the National Centers for Environmental Prediction operational mesoscale Eta model. *Journal of Geophysical Research: Atmospheres*, 108(D22). _eprint: https://onlinelibrary.wiley.com/doi/pdf/10.1029/2002JD003296.

Fablet, R., Ouala, S., and Herzet, C. (2018). Bilinear Residual Neural Network for the Identification and Forecasting of Geophysical Dynamics. In *2018 26th European Signal Processing Conference (EUSIPCO)*, pages 1477–1481. ISSN: 2076-1465.

Filipović, N., Brdar, S., Mimić, G., Marko, O., and Crnojević, V. (2022). Regional soil moisture prediction system based on Long Short-Term Memory network. *Biosystems Engineering*, 213:30–38.

Fulton, R. A., Breidenbach, J. P., Seo, D.-J., Miller, D. A., and O'Bannon, T. (1998). The WSR-88D Rainfall Algorithm. *Weather and Forecasting*, 13(2):377–395. Publisher: American Meteorological Society Section: Weather and Forecasting.

Gutman, G. and Ignatov, A. (1998). The derivation of the green vegetation fraction from NOAA/AVHRR data for use in numerical weather prediction

models. *International Journal of Remote Sensing*, 19(8):1533–1543. Publisher: Taylor & Francis _eprint: https://doi.org/10.1080/014311698215333.

Hansen, M. C., Defries, R. S., Townshend, J. R. G., and Sohlberg, R. (2000). Global land cover classification at 1 km spatial resolution using a classification tree approach. *International Journal of Remote Sensing*, 21(6-7):1331–1364. Publisher: Taylor & Francis _eprint: https://doi.org/10.1080/014311600210209.

Hornik, K., Stinchcombe, M., and White, H. (1989). Multilayer feedforward networks are universal approximators. *Neural Networks*, 2(5):359–366.

Jacquemin, B. and Noilhan, J. (1990). Sensitivity study and validation of a land surface parameterization using the HAPEX-MOBILHY data set. *Boundary-Layer Meteorology*, 52(1):93–134.

Jarvis, P. G., Monteith, J. L., and Weatherley, P. E. (1976). The interpretation of the variations in leaf water potential and stomatal conductance found in canopies in the field. *Philosophical Transactions of the Royal Society of London. B, Biological Sciences*, 273(927):593–610. Publisher: Royal Society.

Jin, J., Miller, N. L., and Schlegel, N. (2010). Sensitivity Study of Four Land Surface Schemes in the WRF Model. *Advances in Meteorology*, 2010(1):167436. _eprint: https://onlinelibrary.wiley.com/doi/pdf/10.1155/2010/167436.

Joyce, R. J., Janowiak, J. E., Arkin, P. A., and Xie, P. (2004). CMORPH: A Method that Produces Global Precipitation Estimates from Passive Microwave and Infrared Data at High Spatial and Temporal Resolution. *Journal of Hydrometeorology*, 5(3):487–503. Publisher: American Meteorological Society Section: Journal of Hydrometeorology.

Koren, V., Schaake, J., Mitchell, K., Duan, Q.-Y., Chen, F., and Baker, J. M. (1999). A parameterization of snowpack and frozen ground intended for NCEP weather and climate models. *Journal of Geophysical Research: Atmospheres*, 104(D16):19569–19585. _eprint: https://onlinelibrary.wiley.com/doi/pdf/10.1029/1999JD900232.

Koster, R. D., Mahanama, S. P. P., Yamada, T. J., Balsamo, G., Berg, A. A., Boisserie, M., Dirmeyer, P. A., Doblas-Reyes, F. J., Drewitt, G., Gordon,

C. T., Guo, Z., Jeong, J.-H., Lawrence, D. M., Lee, W.-S., Li, Z., Luo, L., Malyshev, S., Merryfield, W. J., Seneviratne, S. I., Stanelle, T., van den Hurk, B. J. J. M., Vitart, F., and Wood, E. F. (2010). Contribution of land surface initialization to subseasonal forecast skill: First results from a multi-model experiment. *Geophysical Research Letters*, 37(2). _eprint: https://onlinelibrary.wiley.com/doi/pdf/10.1029/2009GL041677.

Kratzert, F., Klotz, D., Brenner, C., Schulz, K., and Herrnegger, M. (2018). Rainfall–runoff modelling using Long Short-Term Memory (LSTM) networks. *Hydrology and Earth System Sciences*, 22(11):6005–6022.

Kratzert, F., Klotz, D., Shalev, G., Klambauer, G., Hochreiter, S., and Nearing, G. (2019). Towards learning universal, regional, and local hydrological behaviors via machine learning applied to large-sample datasets. *Hydrology and Earth System Sciences*, 23(12):5089–5110. Publisher: Copernicus GmbH.

Kumar, S. V., Mocko, D. M., Fadji, M., Hain, C. R., Fuchs, B., and Wade, R. (2024). The North American Land Data Assimilation System (NLDAS-3) Phase 3: Modeling Water Availability over North and Central America.

Lapuschkin, S., Wäldchen, S., Binder, A., Montavon, G., Samek, W., and Müller, K.-R. (2019). Unmasking Clever Hans predictors and assessing what machines really learn. *Nature Communications*, 10(1):1096. Publisher: Nature Publishing Group.

Lees, T., Reece, S., Kratzert, F., Klotz, D., Gauch, M., De Bruijn, J., Kumar Sahu, R., Greve, P., Slater, L., and Dadson, S. J. (2022). Hydrological concept formation inside long short-term memory (LSTM) networks. *Hydrology and Earth System Sciences*, 26(12):3079–3101.

Liang, X., Lettenmaier, D. P., Wood, E. F., and Burges, S. J. (1994). A simple hydrologically based model of land surface water and energy fluxes for general circulation models. *Journal of Geophysical Research: Atmospheres*, 99(D7):14415–14428. _eprint: https://onlinelibrary.wiley.com/doi/pdf/10.1029/94JD00483.

Livneh, B., Xia, Y., Mitchell, K. E., Ek, M. B., and Lettenmaier, D. P. (2010). Noah LSM Snow Model Diagnostics and Enhancements. *Journal of Hydrometeorology*, 11(3):721–738. Publisher: American Meteorological Society Section: Journal of Hydrometeorology.

Mahfouf, J. F. and Noilhan, J. (1991). Comparative Study of Various Formulations of Evaporations from Bare Soil Using In Situ Data. *Journal of Applied Meteorology and Climatology*, 30(9):1354–1365. Publisher: American Meteorological Society Section: Journal of Applied Meteorology and Climatology.

Mahrt, L. and Ek, M. (1984). The Influence of Atmospheric Stability on Potential Evaporation. *Journal of Climate and Applied Meteorology*, 23(2):222–234.

Mahrt, L. and Pan, H. (1984). A two-layer model of soil hydrology. *Boundary-Layer Meteorology*, 29(1):1–20.

Mitchell, K., Helin, W., Lu, S., Gayno, G., and Meng, J. (2005). NCEP implements major upgrade to its medium-range global forecast system, including land-surface component. *GEWEX News*, 15(4):8–9.

Mitchell, K. E., Lohmann, D., Houser, P. R., Wood, E. F., Schaake, J. C., Robock, A., Cosgrove, B. A., Sheffield, J., Duan, Q., Luo, L., Higgins, R. W., Pinker, R. T., Tarpley, J. D., Lettenmaier, D. P., Marshall, C. H., Entin, J. K., Pan, M., Shi, W., Koren, V., Meng, J., Ramsay, B. H., and Bailey, A. A. (2004). The multi-institution North American Land Data Assimilation System (NLDAS): Utilizing multiple GCIP products and partners in a continental distributed hydrological modeling system. *Journal of Geophysical Research: Atmospheres*, 109(D7). _eprint: https://onlinelibrary.wiley.com/doi/pdf/10.1029/2003JD003823.

Mozer, M. C. (1995). A focused backpropagation algorithm for temporal pattern recognition. In *Backpropagation: theory, architectures, and applications*, pages 137–169. L. Erlbaum Associates Inc., USA.

Nash, J. E. and Sutcliffe, J. V. (1970). River flow forecasting through conceptual models part I — A discussion of principles. *Journal of Hydrology*, 10(3):282–290.

Nonnenmacher, M. and Greenberg, D. S. (2021). Deep Emulators for Differentiation, Forecasting, and Parametrization in Earth Science Simulators. *Journal of Advances in Modeling Earth Systems*, 13(7):e2021MS002554. _eprint: https://onlinelibrary.wiley.com/doi/pdf/10.1029/2021MS002554.

O., S. and Orth, R. (2021). Global soil moisture data derived through machine learning trained with in-situ measurements. *Scientific Data*, 8(1):170. Publisher: Nature Publishing Group.

of the Interior, E. R. O. a. S. C. S. G. S. S. D. (1997). USGS 30 ARC-second Global Elevation Data, GTOPO30.

Otkin, J. A., Anderson, M. C., Hain, C., Svoboda, M., Johnson, D., Mueller, R., Tadesse, T., Wardlow, B., and Brown, J. (2016). Assessing the evolution of soil moisture and vegetation conditions during the 2012 United States flash drought. *Agricultural and Forest Meteorology*, 218-219:230–242.

Pan, H.-L. and Mahrt, L. (1987). Interaction between soil hydrology and boundary-layer development. *Boundary-Layer Meteorology*, 38(1):185–202.

Pinker, R. T., Tarpley, J. D., Laszlo, I., Mitchell, K. E., Houser, P. R., Wood, E. F., Schaake, J. C., Robock, A., Lohmann, D., Cosgrove, B. A., Sheffield, J., Duan, Q., Luo, L., and Higgins, R. W. (2003). Surface radiation budgets in support of the GEWEX Continental-Scale International Project (GCIP) and the GEWEX Americas Prediction Project (GAPP), including the North American Land Data Assimilation System (NLDAS) project. *Journal of Geophysical Research: Atmospheres*, 108(D22). _eprint: https://onlinelibrary.wiley.com/doi/pdf/10.1029/2002JD003301.

Rosero, E., Yang, Z.-L., Wagener, T., Gulden, L. E., Yatheendradas, S., and Niu, G.-Y. (2010). Quantifying parameter sensitivity, interaction, and transferability in hydrologically enhanced versions of the Noah land surface model over transition zones during the warm season. *Journal of Geophysical Research: Atmospheres*, 115(D3). _eprint: https://onlinelibrary.wiley.com/doi/pdf/10.1029/2009JD012035.

Rumelhart, D. E., Hinton, G. E., and Williams, R. J. (1986). Learning representations by back-propagating errors. *Nature*, 323(6088):533–536. Publisher: Nature Publishing Group.

Saha, S., Moorthi, S., Wu, X., Wang, J., Nadiga, S., Tripp, P., Behringer, D., Hou, Y.-T., Chuang, H.-y., Iredell, M., Ek, M., Meng, J., Yang, R., Mendez, M. P., Dool, H. v. d., Zhang, Q., Wang, W., Chen, M., and Becker, E. (2014).

The NCEP Climate Forecast System Version 2. *Journal of Climate*, 27(6):2185–2208. Publisher: American Meteorological Society Section: Journal of Climate.

Schaake, J. C., Koren, V. I., Duan, Q.-Y., Mitchell, K., and Chen, F. (1996). Simple water balance model for estimating runoff at different spatial and temporal scales. *Journal of Geophysical Research: Atmospheres*, 101(D3):7461–7475. _eprint: https://onlinelibrary.wiley.com/doi/pdf/10.1029/95JD02892.

Wei, H., Xia, Y., Mitchell, K. E., and Ek, M. B. (2011). Improvement of the Noah land surface model for warm season processes: evaluation of water and energy flux simulation. *Hydrological Processes*, 27(2):297–303. _eprint: https://onlinelibrary.wiley.com/doi/pdf/10.1002/hyp.9214.

White, A. T., White, K. D., Hain, C. R., Antia, M., Fuell, K., and Case, J. L. (2025). NASA SPoRT's Streamflow-AI: Updates and Advancements. NTRS Author Affiliations: University of Alabama in Huntsville, NOAA National Weather Service, Marshall Space Flight Center, Amentum, Ensco (United States) NTRS Meeting Information: 105th American Meteorological Society (AMS) Annual Meeting; 2025-01-12 to 2025-01-16; undefined NTRS Document ID: 20250000353 NTRS Research Center: Marshall Space Flight Center (MSFC).

Xia, Y., Mitchell, K., Ek, M., Cosgrove, B., Sheffield, J., Luo, L., Alonge, C., Wei, H., Meng, J., Livneh, B., Duan, Q., and Lohmann, D. (2012a). Continental-scale water and energy flux analysis and validation for North American Land Data Assimilation System project phase 2 (NLDAS-2): 2. Validation of model-simulated streamflow. *Journal of Geophysical Research: Atmospheres*, 117(D3). _eprint: https://onlinelibrary.wiley.com/doi/pdf/10.1029/2011JD016051.

Xia, Y., Mitchell, K., Ek, M., Sheffield, J., Cosgrove, B., Wood, E., Luo, L., Alonge, C., Wei, H., Meng, J., Livneh, B., Lettenmaier, D., Koren, V., Duan, Q., Mo, K., Fan, Y., and Mocko, D. (2012b). Continental-scale water and energy flux analysis and validation for North American Land Data Assimilation System project phase 2 (NLDAS-2): 1. Intercomparison and application of model products. *Journal of Geophysical Research: Atmospheres*, 117(D3). _eprint: https://onlinelibrary.wiley.com/doi/pdf/10.1029/2011JD016048.

Appendix A: An Example Appendix

Appendices should appear at the very end of your thesis. Make sure to label each Appendix with a letter starting with "A". Any tables and/or figures located in the appendix should be labeled accordingly. For example, below is figure A.1 because it is the first figure that appears in Appendix A.